Determination of the Anisotropic Permeability of a Carbon Cloth Gas Diffusion Layer through X-ray Computer Micro-Tomography and Single-Phase Lattice Boltzmann Simulation

P Rama, Y Liu, R Chen
Loughborough University

H Ostadi, K Jiang
University of Birmingham

X Zhang
University of Liverpool

Paolo Grassini & co-workers
Seal Spa – SAATI Group

Abstract

An investigation of the anisotropic permeability of a carbon cloth gas diffusion layer (GDL) based on the integration of X-ray micro-tomography and Lattice Boltzmann simulation is presented. The method involves the generation of a 3D digital model of a carbon cloth GDL as manufactured using X-ray shadow images acquired through X-ray micro-tomography at a resolution of 1.74 microns. The resulting 3D model is then integrated with a Lattice Boltzmann single-phase numerical solver in the D3Q19 regime in order to predict three orthogonal permeability tensors when a pressure difference is prescribed in the through-plane direction. The results demonstrate that the simulated through-plane permeability is one order of magnitude greater than the in-plane permeability for the sample imaged and that the corresponding degree of anisotropy for the two orthogonal off-principal directions is 0.22 and 0.27. This compares to a measured value of 0.19. The simulated results are also applied to generate parametric coefficients for the semi-empirical Kozeny-Carman (KC) and Tomadakis-Sotirchos (TS) methods of determining permeability. The results demonstrate that both methods can be tuned in order to capture the non-linear relationship between dimensionless permeability and porosity, with average errors of 13.7 and 12.9% respectively. The current research reveals that by applying the X-ray tomography and LB techniques in a complementary manner, there is a strong potential to gain a deeper understanding of microscopic fluidic phenomenon in

representative models of porous fuel cell structures and how this can influence macroscopic transport characteristics which govern fuel cell performance.

Keywords
X-ray, micro-tomography, Lattice Boltzmann, fuel cell, gas diffusion layer, carbon cloth, anisotropy, permeability

1 Introduction

The polymer electrolyte fuel cell (PEFC) is well-poised to play a leading role in the portfolio of future energy technologies. With its potential to operate as a reliable zero emissions energy conversion device which does not combust fuels directly, it is theoretically unbound by the Carnot limit and has the potential to contribute towards reducing urban air pollutants. However, in order to realise its full potential, a detailed understanding is required of the mass transport processes that occur within the micro and nano-structures of the PEFC.

The purpose of this study is to report a technique which merges X-ray micro-tomography to generate direct three-dimensional digital models of heterogeneous porous structures of gas diffusion layers (GDL) with lattice Boltzmann (LB) modelling to simulate single-phase porous flow. The objective of this study is to present research focused at applying the technique to characterise the woven carbon cloth GDL.

The literature demonstrates that the LB technique has been increasingly exploited over the past couple of years to characterise fluidic behaviour through porous fuel cell layers. Nabovati *et al.* [1] and Hao *et al.* [2] recently demonstrated the application of a single-phase LB treatment to simulate anisotropic permeability in stochastically generated 3D models of the carbon paper GDL. Nabovati *et al.* examined the effects of microscopic structural features of individual carbon fibrils on the permeability of the macroscopic material, concluding that fibrils with an aspect ration of less than 6:1 had a tendency to influence permeability [1]. Hao *et al.* compared the simulated permeability of a carbon paper GDL to measurement and to the calculated permeability using the Kozeny-Carman (KC) equation, reporting close

correlation with measurement and calculated results from the KC equation in the through-plane direction [2].

Other studies have focused on the application of the two-phase LB treatment to simulate the behaviour of liquid water through porous fuel cell structures. Niu *et al.* considered the effects of pressure drop, wettability and viscosity ratio on water-gas transport, noting faster transport in the non-wetting phase with a contact angle of 105° compared to 120° [3]. Koido *et al.* focus on validating the predicted capillary-pressure saturation relationship with measurement below a liquid saturation of 0.1, and demonstrated that the LB technique could indeed replicate its general form [4]. Tabe *et al.* investigated liquid water infiltration in 2D using a simplified geometry, concluding that the wettability of the channel can influence two-phase flow through the GDL [5]. Wang *et al.* have studied two-phase phenomenon in a similar vein [6,7]. Their studies have identified that the movement of liquid water can occur through finger-like liquid waterfronts and concluded that liquid coverage at the channel-GDL interface can cause pressure to build up within the GDL and force liquid water through to the surface in preferential locations.

The carbon cloth GDL has been studied much more rarely in the literature. Park *et al.* applied the LB technique to simulate single-phase flow through a single tow section comprised of multiple carbon fibres [8]. They considered flow parallel and perpendicular to the fibre direction, and highlighted that the tow diameter is a critical parameter for permeability in both cases. Van Doormaal *et al*. carried out a similar study which considered whole fibre sections arranged with defined angles and with random orientation [9]. Their study concluded that sample porosity strongly influences both in- and through-plane permeability. It was shown that an anisotropic microstructure would also result in anisotropic permeability.

The LB technique has also been applied elsewhere to characterise flow through porous electrodes in both molten carbonate [10] and solid oxide fuel cells [11,12,13].

While the above review is by no means exhaustive, it highlights the potential of the LB technique to elucidate micro- and nano-scopic fluid flow phenomenon in

the PEFC, which due to the restrictive length scales involved is otherwise formidable. However, one fundamental limitation of all of the PEFC models discussed above as well as other studies is the fact that they all employ stochastic techniques to reconstruct digital 3D models of the carbon paper or carbon cloth GDL [14, 15]. In order to bring the simulations closer towards reality, it is necessary to generate 3D models that are based on the actual microstructure of GDLs as manufactured. In a recent study, the authors demonstrated the application of X-ray micro-tomography to generate a direct 3D model of the carbon paper [16]. The 3D model was then applied with a single-phase lattice Boltzmann model in the D3Q19 scheme to simulate through-plane permeability for validation purposes. In the current study, the authors extend the application of the technique to simulate anisotropic permeability through a carbon cloth GDL.

2 Methodology

The approach applied for this study is characterised by three fundamental components. The first is the LB numerical model, which predicts the permeability of a porous material in three perpendicular directions when the flow is oriented in a primary flow direction. For the purposes of the current research, the primary flow direction is set parallel to the through-plane direction. The second component is the X-ray tomography technique which is applied non-invasively to generate a direct digital 3D model of the porous material. The final component is the experimental technique which is applied to determine the degree of anisotropy of the porous material for validation and analysis purposes. Each is discussed here.

2.1 Principal Equations of the Single-Phase Lattice Boltzmann Numerical Model

In this work, the single-time relaxation LB model is used to simulate single-phase flow through a porous medium [23]. The movement of a fictitious particle is described in terms of the particle distribution function, $f_i(\boldsymbol{x},t)$, which defines the redistributed mass of a particle based on its spatio-temporal history*:*

$$f_i(\boldsymbol{x}+\boldsymbol{\xi}_i\delta t, t+\delta t) = f_i(\boldsymbol{x},t) + \frac{1}{\tau}\left[f_i^{eq}(\boldsymbol{x},t) - f_i(\boldsymbol{x},t)\right] \quad [1]$$

where $\boldsymbol{\xi}_i$ is the velocity in the direction *i*, δt is the time step and $\tau = \delta t/\lambda$ is a dimensionless relaxation time parameter. A particle with velocity $\boldsymbol{\xi}_i$ at location $\boldsymbol{x}$ and time t will redistribute to $\boldsymbol{x}+\boldsymbol{\xi}_i\delta t$ at time $t+\delta t$ after colliding with other particles at location $\boldsymbol{x}$ moving with dissimilar velocities. In the current work, nineteen dissimilar velocities are considered according to the D3Q19 scheme, which are defined as follows: stagnation at the location $\boldsymbol{x}$, (0, 0, 0)/δt, two velocities in the *x* direction (±δx, 0, 0)/δt, two in the *y* direction (0, ±δx, 0)/δt, two in the *z* direction (0, 0, ±δx)/ δt, four in the *x*-*y* plane (±δx, ±δx, 0)/δt, four in the *x*-*z* plane (±δx, 0, ±δx)/δt, and four in the *y*-*z* plane (0, ±δx, ±δx)/δt, where δx is the element length. This is shown in Figure 3.

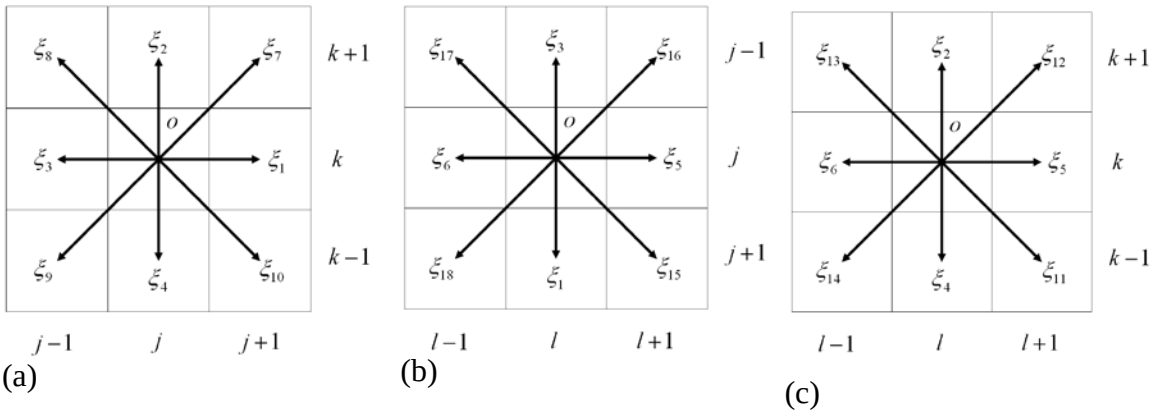

Figure 3

The nineteen velocities in the D3Q19 scheme; (a) the x-y plane; (b) z-x plane; (c) z-y plane.

It is assumed that gas flow is incompressible and restricted to the void space in the GDL. The void-solid interface is assumed to be a non-slip boundary for viscous gases where the gas velocity is zero. In the LB model, the equilibrium distribution function $\boldsymbol{f}_i^{eq}(\boldsymbol{x},\boldsymbol{t})$ depends only on gas density and gas velocity $\boldsymbol{u}$ at location $\boldsymbol{x}$ and time $\boldsymbol{t}$. For incompressible flow, the following equilibrium distribution function proposed by He and Luo [17] is used;

$$f_i^{eq}(\boldsymbol{x},t) = w_i\left\{\rho + \rho_0\left[\frac{\boldsymbol{\xi}_i\cdot\boldsymbol{u}}{c_s^2} + \frac{1}{2}\left(\frac{\boldsymbol{\xi}_i\cdot\boldsymbol{u}}{c_s^2}\right)^2 - \frac{\boldsymbol{u}\cdot\boldsymbol{u}}{2c_s^2}\right]\right\} \quad [2]$$

where w_i is a weighting factor ($w_0 = 1/3$ for $|\xi_i| = 0$, $w_i = 1/18$ for $|\xi_i| = \delta x/\delta t$ and $w_i = 1/36$ for $|\xi_i| = \sqrt{2}\,\delta x/\delta t$), $\boldsymbol{c_s}$ is sound speed, and ρ and $\boldsymbol{u}$ are gas density and gas velocity respectively and are calculated from;

$$\rho = \sum_i \boldsymbol{f_i} = \sum_i \boldsymbol{f_i^{eq}} \quad [3]$$

$$\rho_0\boldsymbol{u} = \sum_i \boldsymbol{f_i}\boldsymbol{\xi_i} = \sum_i \boldsymbol{f_i^{eq}}\boldsymbol{\xi_i} \quad [4]$$

in which ρ_0 is a reference density and assumed to equal unity.

To solve the void-solid boundary, the bounce-back method has been employed where it is assumed that any particle that hits a solid wall during the streaming step simply bounces back to its original position. Since the bounce-back by the wall changes the directions of the particles, they will move in the reverse directions at the end of each time step.

In the LB model, gas flow is driven by an applied pressure difference on two opposite sides of the image along the through-plane direction. The remaining four sides at in-plane directions are treated as non-mirrored periodic boundaries, in which two opposite sides are neighboured such that particles moving out of the domain from one side re-enter the domain through its opposite side. Simulations commence from a zero velocity field and the pressure field is linearly distributed in the direction along which the pressure difference is imposed. In order to determine if steady-state conditions have been reached the tolerance denoted Ω is calculated where;

$$\Omega = \frac{\sum_i \left|u_j(x_i, t+100) - u_j(x_j, t)\right|}{\sum_i \left|u_j(x_i, t)\right|} \quad ;(j=x, y, z) \quad [5]$$

Flow is assumed to have reached steady state when the tolerance is less than 10^{-5}.

2.2 Permeability Calculation

The current study focuses on simulating the anisotropic permeability to determine the degree of anisotropy of the GDL and comparing this to that obtained from pressure drop measurements using an air tester. The degree of anisotropy in the off-principal direction (j) relative to the principal flow direction (i) can be calculated as:

$$\chi = \frac{k_{ij}}{k_{ii}} \qquad [6]$$

The numerical and experimental methods by which the permeability values can be determined are explained here.

2.2.1 Numerical

The permeability of a GDL is calculated from the simulated velocity distribution at microscopic scale in the void space of the porous material. The absolute permeability of the GDL, k, at a macroscopic scale can be calculated using Darcy's law. The permeability can be treated as a second-order tensor with six components (k_{ij}, i, j=x, y, z and k_{ij}=k_{ji}), which can all be calculated by applying the pressure difference in different directions of the image. For the purposes of this study, when the pressure difference is applied in the x direction parallel with the through-plane direction, the following three components of the permeability tensor can be calculated such that;

$$k_{xi} = \frac{\rho \mu q_i}{\left(\Delta P / L_x\right)} \qquad [7]$$

where q is the average gas velocity through the GDL in the direction of the pressure-gradient when flow reaches steady state, ρ is the gas density as calculated from Eq. 3,

μ is the kinematic viscosity, ΔP is the applied pressure gradient across the image along the through-plane direction and *i* denotes the off-principal *y* or *z* directions. A full description of the LB model is provided elsewhere [16,[18],[19]].

2.2.2 Experimental

The absolute permeability of the GDL sample can be calculated using Eq. 7, where the through-plane volumetric flow rate is replaced with a measured value for a given pressure drop. A permeability tensor for the principal flow direction and one for the off-principal direction are determined to calculate the degree of anisotropy. The measurements are taken with a Texas Instrument FX 3300 at room temperature using a 20cm^2 sample taken from the same batch as that used for the X-ray imaging process. The carbon cloth employed has a nominal thickness of 377 microns under a compression of 11.37 kPa, warp-weft of approximately 24 threads/cm and a density of 316 kg/m^3. The material does not contain a micro-porous layer (MPL).

2.3 X-Ray Micro-Tomography

The X-ray tomography imaging and direct 3D reconstruction procedure has three basis steps; image acquisition, image processing and finally digital reconstruction. A summarised description of the full procedure [[20],[21]] is provided here.

Image Acquisition via X-ray Micro-Tomography

In order to generate a model of the true heterogeneous porous structure of the GDL in 3D, a set of two-dimensional X-ray shadow images of the GDL are taken by placing the sample in front of an X-ray source and progressively rotating it by 0.9 degrees. The rotation is carried out through a total angle of 180°, resulting in 200 shadow images. In this initial study of the carbon cloth GDL, the sample is imaged as manufactured without any special pre-treatment. Micro-tomography images are then generated using a Skyscan 1072 system, which has an X-ray source of 50 kV at 100 μA. Images are acquired using a Hamamatsu X-ray camera which contains a

scintillator and a charge coupled device (CCD) chip that has a 1024 × 1024 pixel resolution with a 12-bit depth. The object diameter is 1.8 mm resulting in a maximum resolution of 1.74 μm. The principle of the image acquisition process is illustrated in Fig. 2.

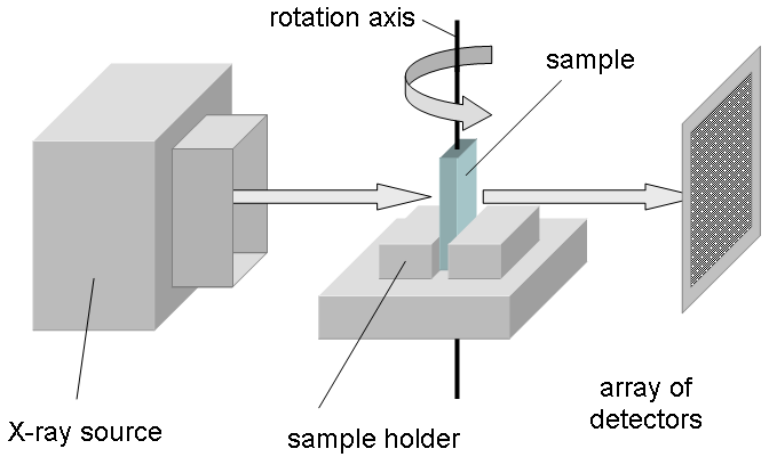

Figure 2

Principle of the micro-tomography system

Image Processing via Heuristic Thresholding

Following the image acquisition step, the 2D greyscale images generated using X-ray tomography are compiled using CTAN software in order to generate a stack of 2D cross-sectional images in a greyscale format (256 shades of grey). In order to then distinguish between solid and void regions in each image, a heuristic thresholding process is be applied which in return results in a stack of binary images where 1 represents solidity and 0 represents void space. In the thresholding process, the average fibre diameter determined from a 2D image of the GDL surface obtained using scanning electron microscopy (SEM) at 1.76 μm resolution is compared to that obtained from a thresholded 2D greyscale surface image generated using CTAN in the preceding step. The threshold applied to the greyscale image is tuned until the resulting average fibre diameter matches that of the SEM image and, by visual inspection, the fibre continuity in the thresholded image is preserved relative to the SEM image. The correct threshold is subsequently applied to the entire stack of greyscale images.

Digital 3D Reconstruction

With the stack of thresholded 2D images, a complete 3D digital model of the GDL is generated using computer algorithms. There are several algorithms that can be applied in order to do this, including Double Time Cubes and Matching Cubes [22]. The resulting 3D model can then be used directly with the LB model without modification to simulate flow through its porous structure. Each binary element in the 3D model represents a voxel which is equal to $1.74 \times 1.74 \times 1.74\ \mu m^3$ in volume.

2.4 Simulation

In the current work, the spatial resolution of the LB model is matched appropriately with the resolution of the 3D image, the porosity of the 3D structure and the computational resources available. The carbon cloth GDL employed in this study has a porosity of greater than 80%, which allows the spatial resolution of the LB model to be set equal to the spatial resolution of the 3D digital model. In the work presented here, the overall model of the GDL generated via X-ray tomography is divided into 21 digital regions. The LB solver is applied to each region to determine the detailed gas velocity field in the porous network of the GDL when it is infiltrated by air, treating each region as its own entity. Because the absolute permeability represents the linear dependence of the volumetric gas flow rate on the pressure drop across the material, it must be ensured that the pressure drop applied in the simulation also corresponds to this linear region. As such, the LB simulations were conducted with an applied pressure differential of 20 Pa. The literature suggests that pressure drops across a GDL under fuel cell operating conditions would be less than 100 Pa [23].

The numerical simulations are carried out on a quad-core 2.33 GHz workstation with 3.25 Gbytes of RAM; an LB simulation for one of the 21 regions requires around 4 hours.

3 Results

3.1 Digital 3D Model

The overall 3D shadow image of the carbon cloth GDL in the *x*-*z* plane and the division into 21 regions is shown in figure 3. The size of each region in voxels is 254 × 254 × 128 (x,y,z) which corresponds to 442 μm × 442 μm × 223 μm. The principal flow direction in the LB simulations is set parallel to the through-plane *y*-direction.

In the current work, the average fibre diameter $\left(d_f\right)$ measured from the SEM reference image is 7.8 μm, which compares to 8 μm from the same surface of the 3D digital model; the error in the average fibre diameter as a result of threshold tuning is therefore 2.6% in magnitude.

Figure 3 3D image of the GDL image with 21 regions of interest

3.2 Simulated Permeability

Figures 4 (a) – (c) show the simulated permeability when the pressure differential is applied in the principal through-plane flow direction (y-direction) and the simultaneous permeability in the off-principal in-plane directions (*x* and *z* directions).

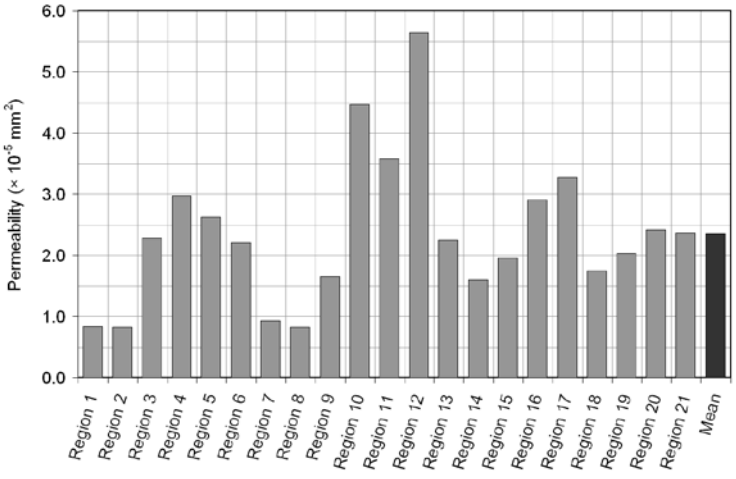

(a)

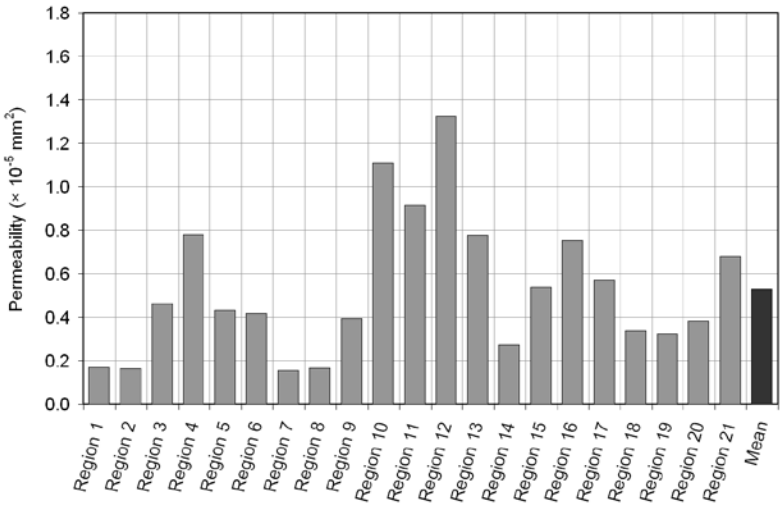

(b)

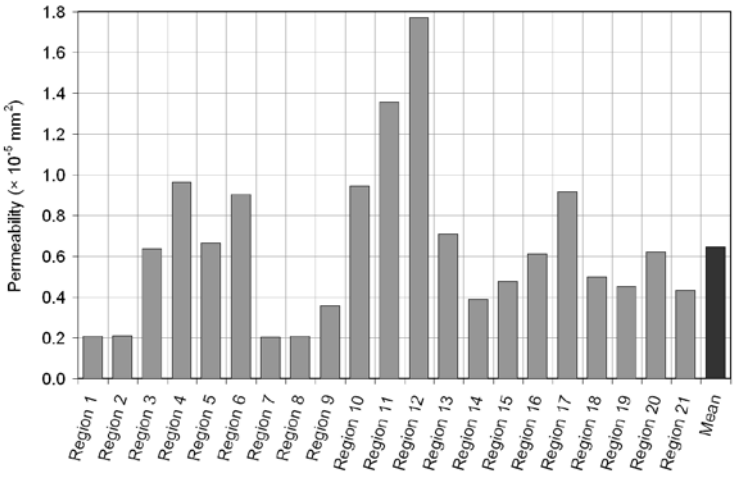

(c)

Figure 4 Simulated absolute permeability through 21 regions of the carbon cloth GDL; (a) principal through plane *y*-direction; (b) off-principal in-plane *x*-direction; (c) off-principal in-plane *z*-direction

The calculated mean absolute permeability of the 21 regions for the through-plane direction is 2.35×10^{-5} mm^2, as shown in Fig. 4a. This compares to 0.53×10^{-5} mm^2 and 0.65×10^{-5} mm^2 in the off-principal in-plane *x* and *z* directions shown in Figs. 4b and 4c respectively. The results therefore demonstrate that for this sample of carbon cloth, the through-plane permeability is one order of magnitude greater than that in the off-principal in-plane directions when the pressure drop occurs through the *x*-*z* plane.

All three sets of results also demonstrate a certain degree of variability in the simulate permeability along each direction. In terms of through-plane permeability, the standard deviation of the simulated results is 1.21×10^{-5} mm^2 and the mean value is

2.35×10^{-5} mm^2, with region 12 having highest permeability of 5.64×10^{-5} mm^2 and region 8 having the lowest of 0.82×10^{-5} mm^2. For in-plane permeability in the *x*-direction, the standard deviation is 0.40×10^{-5} mm^2 and the mean value is 0.53×10^{-5} mm^2. Again, region 12 exhibits the highest in-plane permeability of 1.33×10^{-5} mm^2 compared to the lowest which in this case occurs for region 7, being 0.15×10^{-5} mm^2. Figure 4c demonstrates similar characteristics, where the standard deviation is 0.32×10^{-5} mm^2 and the mean value is 0.65×10^{-5} mm^2. Regions 12 and 7 again exhibit highest and lowest permeabilities of 1.77×10^{-5} mm^2 and 0.20×10^{-5} mm^2 respectively. Figures 5 a-c enables a closer inspection of the structural features of Regions 7, 8 and 12.

Figures 5a and 5b illustrate that in regions 7 and 8, two carbon fibre tows overlap one another, resulting in a regular weave. This tight arrangement results in the low permeabilities discussed above. Figure 5c on the other hand shows a large void in region 12. Figure 6a shows that region 12 corresponds to an area that lies where four orthogonal carbon fibre tows intersect. The resulting void space, which is exposed fully in figure 6b, results in less obstruction to gas transport and therefore higher permeability.

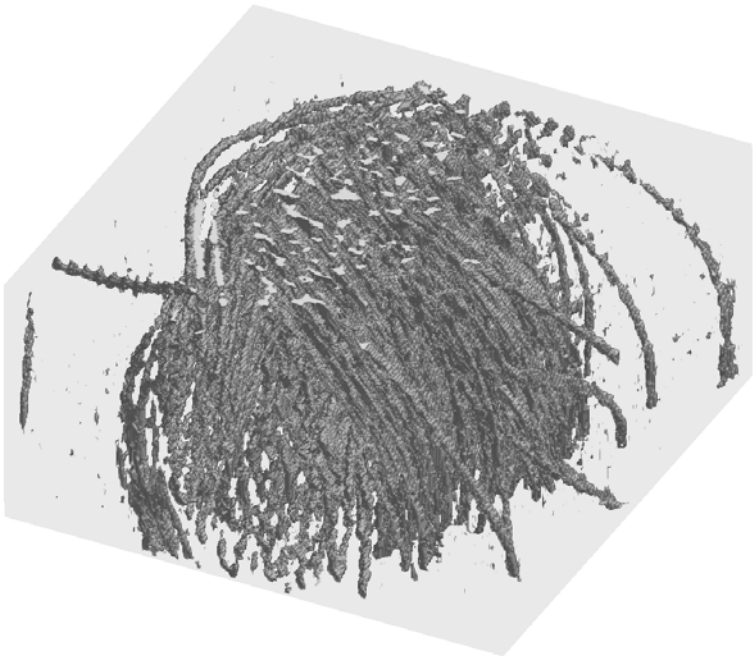

(a)

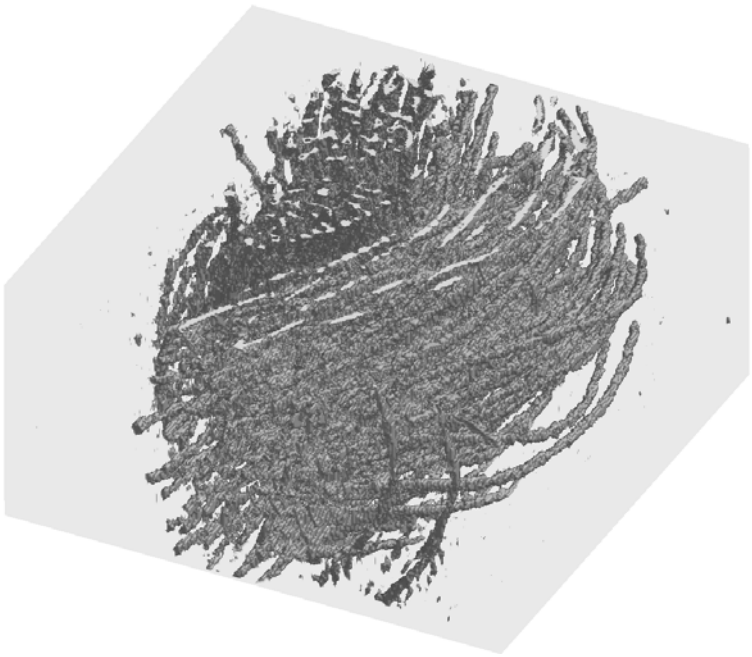

(b)

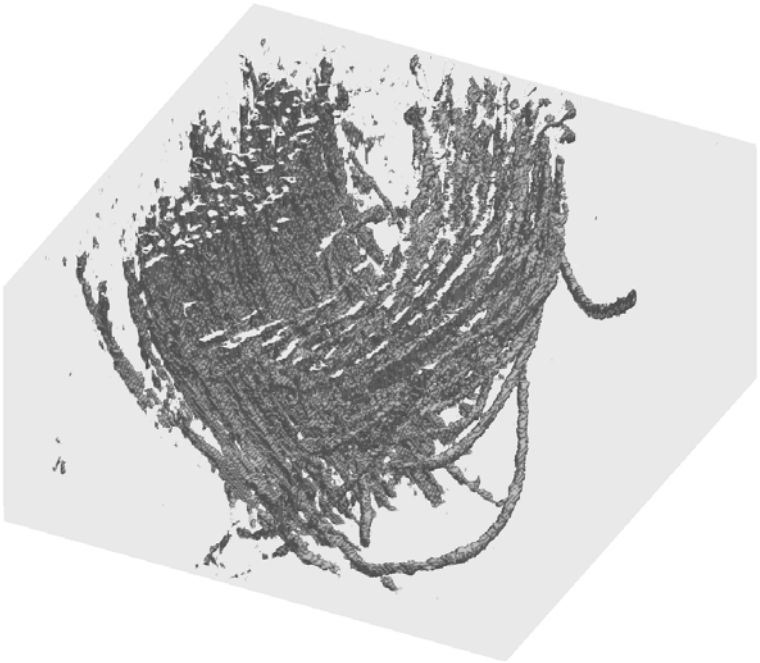

(c)

Figure 5 Binary images of (a) region 7, (b) region 8 and (c) region 12

The relatively low values of permeability calculated in through- and in-plane directions for regions 1 and 2 can be explained in the same manner; the dense weave patterns in these regions result in low absolute permeability whereas regions 5 and 6 contain large void regions where tows intersect, resulting in high absolute

permeability. The results therefore suggest a dependence of permeability on the porosity of each region.

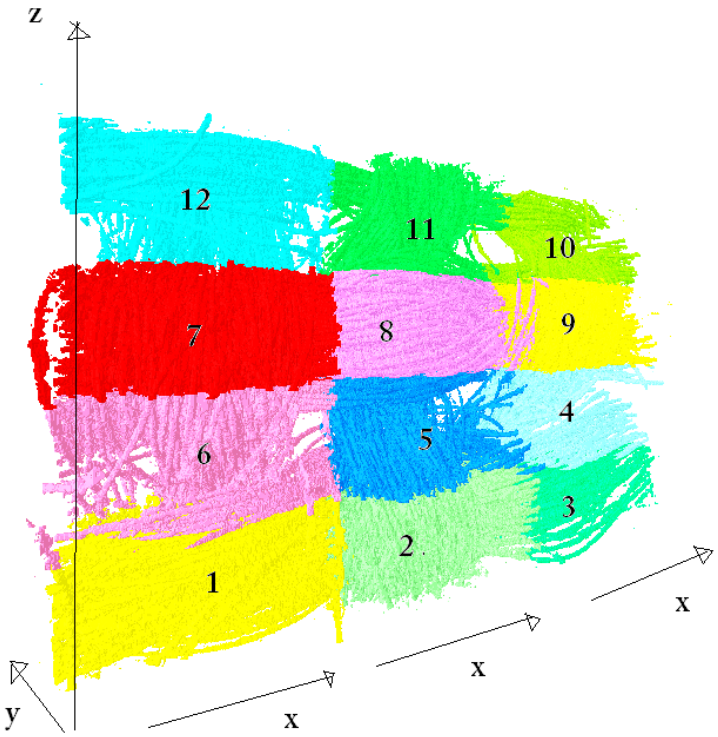

(a)

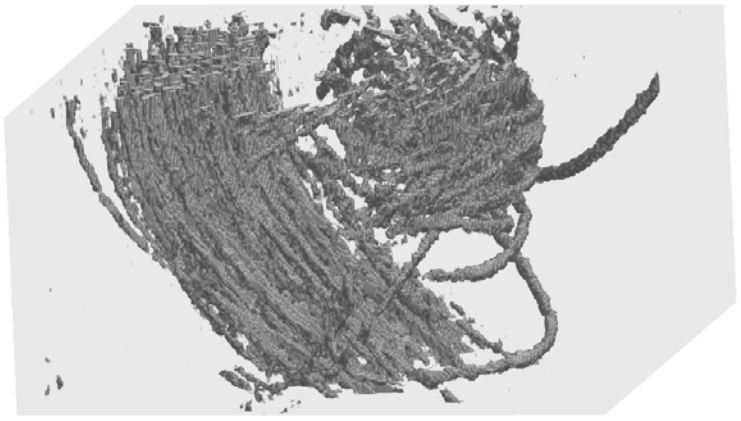

(b)

Figure 6 Void regions between four intersecting tows of (a) entire 3D model, (b) region 12

The relationship between porosity and permeability for this sample of carbon cloth is elucidated by Figure 7, where each data point corresponds to one of the 21 regions in the digital model. In general, the results show that the porosity of each

region is within the band of 0.910 to 0.955. The three lines of best fit show that the increase in permeability over the same range from a minimum value of 0.8 $\times 10^{-5}$ mm^2 is 3.2$\times 10^{-5}$ mm^2 for the principal flow direction. In the off-principal direction, the increase in permeability from the minimum value of around 0.2 $\times 10^{-5}$ mm^2 is 0.8$\times 10^{-5}$ mm^2. The results therefore suggest that the if the local weave structure results in a 5% increase in porosity, the permeability tensor can increase by as much as 400% in both the through-plane and in-plane directions.

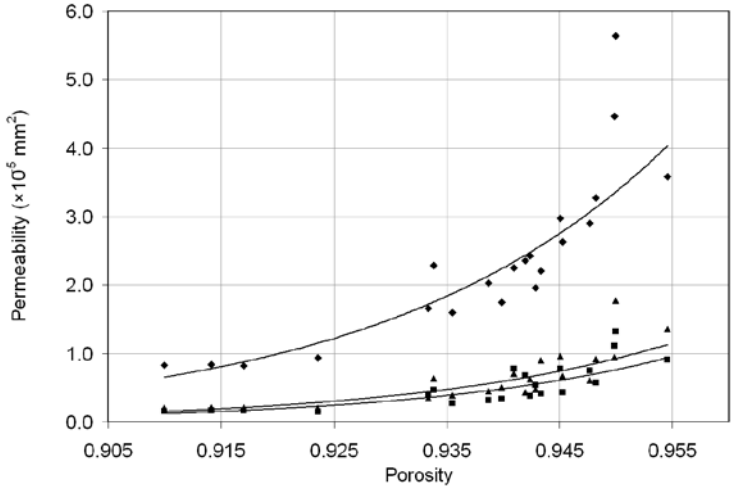

Figure 7 Calculated absolute permeability of 21 regions as a function of region porosity for (♦) through-plane permeability in the principal y-direction, (■) in-plane permeability in the off-principal x-direction, (▲) in-plane permeability in the off-principal z-direction

3.3 Degree of Anisotropy

Anisotropic permeability can be a key factor in the selection of porous materials for fuel cell applications, particularly for cells employing interdigitated flow field designs. Figure 8 shows the calculated degree anisotropy in the off-principal *x* and *z* directions using the data presented in Figure 5. The average degree of anisotropy in the x-direction relative to y-direction is 0.22. For the z-direction, the average is 0.27. The degree of anisotropy based on experimental measurements is 0.19. Generally speaking, therefore the simulated results compare well to measured data for the carbon cloth GDL.

Inspection of the results reveals that the greatest degree of anisotropy occurs in regions which are in the vicinity of or contain void regions between four intersecting tows. For example, figure 8b identifies regions 6 and 11 as those where the anisotropy exceeds 0.35. Figure 6a again confirms that the void spaces between intersecting tows which run along specific directions in these regions will allow air to pass through preferential pathways. Part of the flow approaching regions 6 and 11 perpendicular to the *x*-*z* plane is deflected in the direction of regions 1 and 8 respectively, which in return results in greater permeability for regions 6 and 11 in the *z*-direction relative to the *x*-direction. This is shown in figure 8b.

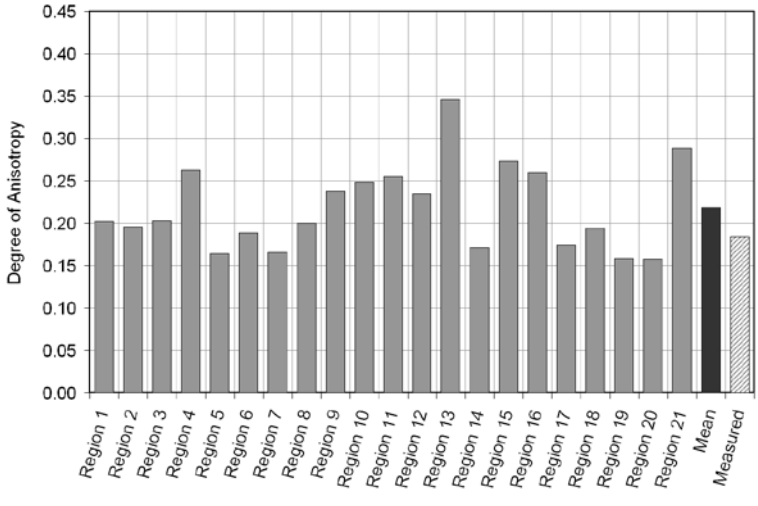

(a)

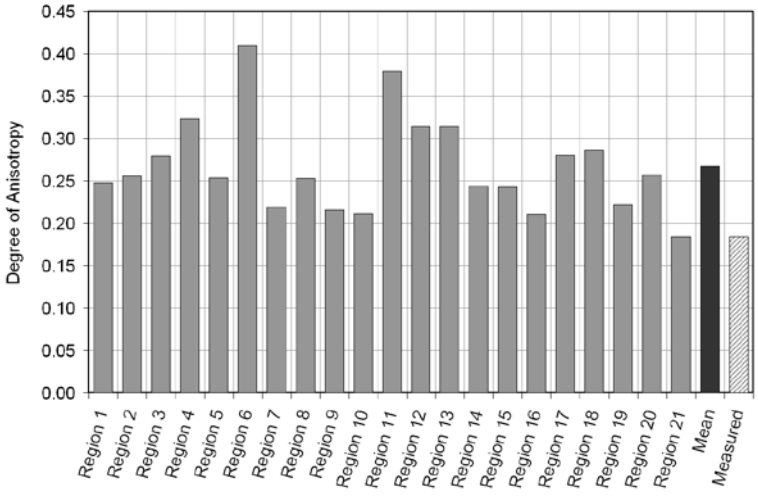

(b)

Figure 8 Calculated degree of anisotropy (a) in the off-principal *x* direction and (b) in the off-principal *z* direction

3.4 Permeability Prediction

The literature demonstrates that the through-plane permeability of porous fuel cell media can be determined using semi-empirical means such as the Carman-Kozeny (KC) and the Tomadakis-Sotirichos (TS) methods [24]. Either of these can be easily incorporated into multi-layer macroscopic fuel cell models for cell simulation but rely upon pre-requisite knowledge of parametric coefficients based on the structure of the porous medium. Using the through-plane permeability data presented in Figure 7 and the average fibre diameter, it is possible to fit both the KC and TS curves to the simulated LB data by tuning their respective parametric coefficients.

The KC model can be expressed as follows to give the dimensionless permeability [24];

$$\frac{k}{r^2} = \frac{\varepsilon^3}{4K_{KC}(1-\varepsilon)^2} \qquad [8]$$

where ε is the material porosity, r is the average fibre radius and K_{KC} is the KC constant which depends on fibre alignment and arrangement. Since the porosity of each region is already known from the LB simulations, it is possible to tune just the KC constant. The TS model is based on a more comprehensive treatment [25] and can be expressed as;

$$\frac{k}{r^2} = \frac{\varepsilon}{8\ln^2\varepsilon}\frac{(\varepsilon-\varepsilon_p)^{\alpha+2}}{(1-\varepsilon_p)^{\alpha}\left[(\alpha+1)\varepsilon-\varepsilon_p\right]^2} \qquad [9]$$

where ε_p is the percolation threshold and α is a constant which depends on the structure and the flow direction. In this case, both ε_p and α have to be tuned. The percolation threshold represents a porosity at which infinite connectivity is established in the void spaces and mass transport is initiated through the porous structure.

For both the KC and TS methods, the parametric coefficients are tuned until the average error for all data points reaches its minimum value relative to the 21

simulated dimensionless permeabilities from the LB model. Figure 8 compares the KC and TS predictions to results from the LB model. Again, each data point from the LB model represents one of the 21 regions of interest in the 3D digital model.

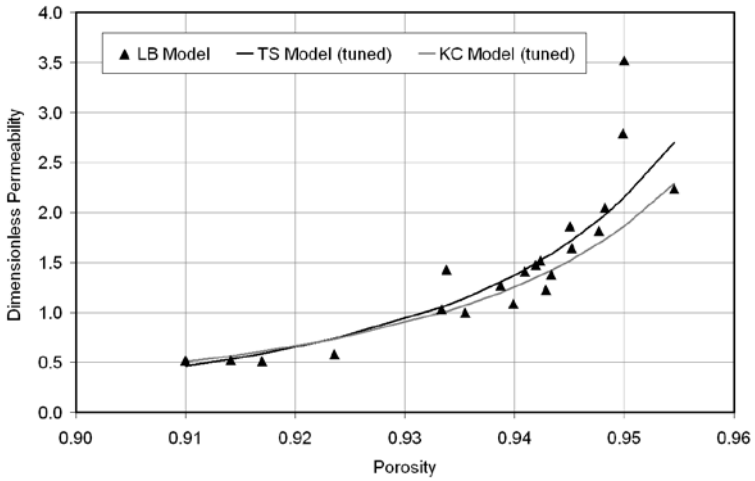

Figure 8 Comparison of simulated permeability using the LB model to the predictions of the KC and TS models with tuned parametric coefficients

The results show that both the TS and KC methods are generally capable of capturing the dependence of through-plane dimensionless permeability on porosity for the carbon cloth material analysed in this study. In the KC method, the KC constant is tuned to a value of 46, which results in an average error of 13.7%. It is difficult to ascertain if the precise magnitude of this value is reasonable given the lack of data for carbon cloth GDLs. It is approximately 33 times that reported for E-Tek Cloth 'A' by Gostick *et al.* [24], however, in the general context of gas diffusion media could be viable as it is 1.7 times that reported for Ballard P75 by the same authors which also exhibits anisotropic permeability and strongly aligned fibres [24]. In addition, the literature suggests that the KC constant is expected to be high for materials with a porosity greater than 0.8, which is indeed the case for the carbon cloth sample analysed here [[26]]. In the case of the TS method, the threshold percolation is set to a value of 0.60 while α is set to a value of 1.19, which results in an average error of 12.9%. The literature provides values in the range of 0.037 – 0.33 for the threshold percolation and 0.521 – 1.099 for the parameter α although these parameters are primarily for randomly overlapping fibres [25,[27]]. The literature suggests that the threshold percolation approaches 0.33 for partially overlapping fibre structures [[28]]. In

the case of carbon cloth the tows fully overlap due to the regular weave structure and as such it can be presumed that the percolation threshold could correspondingly increase. The literature also suggests that the parameter α can be estimated as follows for fully overlapping fibres [28]:

$$\alpha = 2.28\varepsilon_p + 0.35 \qquad [10]$$

Substituting the value of 0.60 for ε_p yields a value of α of 1.718; the tuned figure of 1.099 is well-within this value.

4 Conclusions and Discussion

The brief study presented in this research has demonstrated the potential to generate representative digital 3D models of the carbon cloth GDL based on X-ray micro-tomography and to simulate anisotropic permeability through its porous structure through single-phase LB simulations. The following conclusions can be drawn from the current work:

1. Direct digital reconstruction of the carbon cloth GDL using X-ray micro-tomography and integration with a single-phase 3D Lattice Boltzmann numerical solver. The three-step image acquisition, image processing and model generation process described in this study has successfully demonstrated the ability to generate a representative 3D model of a carbon cloth GDL using X-ray micro-tomography. In this work, the resolution of the acquired image is 1.74 μm. The threshold tuning processes currently employed results in a 2.6% error in the average fibre diameter of the generated model, relative to that determined from an SEM image taken at a resolution of 1.76 μm. The study also demonstrates that the digital 3D model of the GDL can be applied with a 3D single-phase Lattice Boltzmann numerical solver in order to simulate microscopic flow through its porous structure.

2. Simulation of anisotropic permeability. The numerical results from the LB model demonstrate that the mean absolute permeability in the principal flow direction for the analysed carbon cloth sample is 2.35×10^{-5} mm^2, and 0.53×10^{-5} mm^2 and 0.65×10^{-5}

mm^2 respectively in the off-principal *x* and *z* directions. The degree of anisotropy is calculated as the ratio of the predicted absolute permeability in the off-principal directions to that in the principal flow direction. The results show that the degree of anisotropy is 0.22 and 0.27 for the x-to-y and z-to-y directions respectively. This shows acceptable agreement with the experimental value of 0.19. The numerical results also show that the degree of anisotropy in carbon cloth GDLs is influenced by the local weave structure and the presence of void sections where four orthogonal tows intersect.

3. Comparison with KC and TS methods to predict permeability. The semi-empirical KC and TS equations have been fitted to the simulated permeability curves generated by the LB model in order to elucidate parametric coefficients that have otherwise been largely unreported in the literature for carbon cloth GDLs. The results demonstrate that both methods are capable of replicating the general relationship between porosity and dimensionless permeability in the porosity range of 0.91 to 0.955. The average errors for the two methods are 13.7% and 12.9% respectively. The simulations suggest that for the carbon cloth considered, the KC constant is 46, while the threshold percolation and α for the TS model are 0.60 and 1.099 respectively.

The imaging process employed in the current work does not involve any sample preparation steps. As such, the GDL is imaged in its freely expanded natural state. It is acknowledge that under fuel cell stack conditions, the compaction pressure applied to hold the stack together and seal the peripheries would alter the compactness of carbon fibre tows and therefore its geometric structure. Current work is focusing on developing a basic sample preparation technique to permanently pre-compress the GDL under representative compaction forces in order to investigate the effect of cell compression of the flow characteristics of the porous material.

5 Acknowledgements

This research was supported by the UK Technology Strategy Board (TSB Project No.: TP/6/S/K3032H). We acknowledge industrial partners AVL List GmbH, Intelligent Energy Ltd., Johnson Matthey Fuel Cells Ltd., Saati Group Inc. and Technical Fibre Products Ltd. for their support of this work.

6 References

[1] Nabovati A, Lllwellin EW, Suosa ACM. **A general model for the permeability of fibrous porous media based on fluid flow simulations using the lattice Boltzmann method.** Composites: Part A. 2009, 40, 860-869

[2] Hao L, Cheng P. **Lattice Boltzmann simulations of anistropic permeabilities in carbon paper gas diffusion layers.** J. Power Sources, 2009, 186, 104-114

[3] Niu XD, Munekata T, Hyodo S-A, Suga K. **An investigation of water-gas transport processes in the gas-diffusion-layer of a PEM fuel cell by a mulit-phase multiple-relaxation-time lattice Boltzmann model.** J. Power Sources, 2007, 172, 542-552

[4] Koido T, Furusawa T, Moriyama K. **An approach to modeling two-phase transport in the gas diffusion layer of a proton exchange membrane fuel cell.** J. Power Sources, 2008, 175, 127-136

[5] Tabe Y. Lee Y, Chikahisa T, Kizakai M. **Numerical simulation of liquid water and gas flow in a channel and a simplified gas diffusion layer model of polymer electrolyte membrane fuel cells using the lattice Boltzmann method.** J. Power Sources, 2009, 193, 24-31

[6] Sinha PK, Wang CY. **Pore-network modeling of liquid water transport in gas diffusion layer of a polymer electrolyte fuel cell.** Electrochimica Acta, 2007, 52, 7936-7945

[7] Mukherjee PP, Wang CY, Kang Q. **Mesoscopic modelling of two-phase behaviour and flooding phenomena in polymer electrolyte fuel cells.** Electrochemical Acta, 2009, *in print*

[8] Park J, Matsubara M, Li X. **Application of lattice Boltzmann method to a micro-scale flow simulation in the porous electrode of a PEM fuel cell.** J. Power Sources, 2007, 173, 404-414

[9] Van Doormaal MA, Pharoah JG. **Determination of permeability in fibrous porous media using the lattice Boltzmann method with application to PEM fuel cells.** Int. J. Numer. Meth. Fluids, 2009, 59, 75-89

[10] Xu YS, Liu Y, Huang GX. **Lattice Boltzmann simulation on molten carbonate fuel cell performance.** J. Electrochem. Soc., 2006, 153(3), A607-A613

[11] Asinari P, Quaglia MC, von Sparkovsky MR, Kasula BV. **Direct numerical calculation of the kinematic tortuosity of reactive mixture flow in the anode layer of solid oxide fuel cells by the lattice Boltzmann method.** J. Power Sources, 2007, 170, 359-375

[12] Joshi AS, Grew KN, Peracchio AA, Chiu WKS. **Lattice Boltzmann modeling of 2D gas transport in a solid oxide fuel cell anode.** J. Power Sources, 2007, 164, 631-638

[13] Suzue Y, Shikazono N, Kasagi N. **Micro modelling of solid oxide fuel cell anode based on stochastic reconstruction.** J. Power Sources, 2008, 184, 52-59

[14] Schulz VP, Becker J, Weigmann A, Mukherjee PP, Wang CY. **Modeling of two-phase behaviour in the gas diffusion medium of PEFCs via full morphological approach.** J. Electrochem. Soc., 2007, 154(4), B419-B426

[15] Theidmann R, Fleishcer F, Hartnig C, Lehnert W, Schmidt V. **Stochastic 3D modeling of the GDL structure in PEMFCs based on thin section detection.** J. Electrochem. Soc., 2008, 155(4), B391-B399

[16] Rama P, Liu Y, Chen R, Ostadi H, Jiang K, Zhang X, Fisher R, Jeschke M. **An X-ray tomography based lattice Boltzmann simulation study on gas diffusion layers of a polymer electrolyte fuel cells.** ASME J. Fuel Cell Sci. Technol., DOI:10.1115/1.3211096, *in press*

[17] He X, Luo L. **Lattice Boltzmann model for the incompressible Navier–Stokes equation.** Journal of Statistical Physics, 1997; 88: 927-948

[18] Zhang X, Crawford JW, Bengough AG, Young IY. **On boundary conditions in the lattice Boltzmann model for advection and anisotropic dispersion equation.** Adv. Water Resour., 2002, 25, 601-609

[19] Zhang X, Ren L. **Lattice Boltzmann model for agrochemical transport in soils.** J. Contam. Hydrol., 2003, 67, 27-42

[20] H Ostadi, K Jiang, PD Prewett. **Micro/nano X-ray tomography reconstruction fine tuning using scanning electron microscope images.** Micro and Nano Letters, 3(4):106-109

[21] H Ostadi, K Jiang, PD Prewett. **Micro/nano X-ray tomography reconstruction tuning using images for PEMFC gas diffusion layers.** Nanotechnology, 2008; 428-431

[22] X Zhang, JW Crawford, AG Bengough, IM Young. **On boundary conditins in the lattice Boltzmann model for advection and anisotropic dispersion equation.** Advances in Water Resources, 2002; 25:601-609

[23] Bevers D, Rogers R, von Bradke M. **Examination of the influence of PTFE coating on the properties of carbon paper in polymer electrolyte fuel cells.** Journal of Power Sources, 1996; 63:193-201

[24] JT Gostick, MW Fowler, MD Pritzker, MA Ioannidis, LM Behra. **In-plane and through-plane permeability of carbon fiber electrode backing layers.** Journal of Power Sources, 2006; 162:228-238

[25] MM Tomadakis, TJ Robertson. **Viscous Permeability of Random Fiber Structures: Comparison of Electrical and Diffusional Estimates with Experimental and Analytical Results.** Journal of Composite Materials, 2005; 39(2):163-188

[26] MJ Matteson, C Orr. **Filtration: principles and practices.** pp 180 Marcel Dekker, INC., New York, 1987

[27] MM Tomadakis, SV Sotirchos. **Effective Knudsen Diffusivities in Structures of Randomly Overlapping Fibers.** AIChE Journal, 1991, 37(1):74-85

[28] MM Tomadakis, SV Sotirchos. **Knudsen Diffusivities and Properties of Structures of Unidirectional Fibers.** AIChE Journal, 1991, 37(8):1175-1186